A stacked memory device on logic 3D technology for ultra-high-density data storage

A stacked memory device on logic 3D technology for ultra-high-density data storage

Jiyoung Kim[1,2]**, Augustin J Hong**[1]**, Sung Min Kim**[1,2]**,**
Kyeong-Sik Shin[1]**, Emil B Song**[1]**, Yongha Hwang**[1]**, Faxian Xiu**[1]**,**
Kosmas Galatsis[1]**, Chi On Chui**[1]**, Rob N Candler**[1]**,**
Siyoung Choi[2]**, Joo-Tae Moon**[2] **and Kang L Wang**[1]

[1] Device Research Laboratory, Department of Electrical Engineering, University of California,
Los Angeles, CA 90095, USA
[2] Advanced Technology Development Team and Process Development Team, Memory R&D
Center, Samsung Electronics Co. Ltd, Korea

E-mail: hbt100@ee.ucla.edu

Abstract
We have demonstrated, for the first time, a novel three-dimensional (3D) memory chip
architecture of stacked-memory-devices-on-logic (SMOL) achieving up to 95% of cell-area
efficiency by directly building up memory devices on top of front-end CMOS devices. In order
to realize the SMOL, a unique 3D Flash memory device and vertical integration structure have
been successfully developed. The SMOL architecture has great potential to achieve tera-bit
level memory density by stacking memory devices vertically and maximizing cell-area
efficiency. Furthermore, various emerging devices could replace the 3D memory device to
develop new 3D chip architectures.

S Online supplementary data available from stacks.iop.org/Nano/22/254006/mmedia

(Some figures in this article are in colour only in the electronic version)

1. Introduction

Over the last few decades, the market for mobile and wireless electronic gadgets has increased tremendously. The availability of low-cost and high-density memory chips has enabled a variety of memory intensive applications that run on those smart devices. Being the key driver behind these low-cost memories with gigabyte capacity, the non-volatile NAND Flash memory has the niche of simple cell structure and small cell size [1–10]. Owing to its noiseless, faster, and more mechanically stable operations, the utilization of NAND Flash memory has been rapidly expanded into the SSD (solid-state drive) market that has begun to threaten the conventional magnetic hard drive market shares [11, 3, 12–15]. As a result of geometric scaling, more Flash memory cells can be packed onto the same chip and at a reduced cost per technology generation. These scaling efforts are, however, fast approaching unsustainable limits such as lithographic

patterning resolution, transistor short-channel effects, and ever increasing interference between adjacent cells [3, 5–8].

In order to achieve much higher-density Flash devices with alleviated scaling problems, 3D cell structures [16–24] and multi-level-cells (MLCs) [25, 3, 5, 26–28, 9] are feasible pathways forward and are currently being developed in nearly all semiconductor memory corporations. MLC chips containing two or three memory bits in a single cell have already been adopted as a standard in consumer electronics. Since the continual increase of MLC memory density has resulted in slower operation and instability during data reading [29–31], the emphasis in research and development is shifting toward the 3D cell approach. Although several 3D structures have been proposed to date, including Bit Cost Scalable (BiCS, figures 1(a)–(c)) from Toshiba [18, 19, 23], their acceptance is restrained by the complex and high-cost fabrication steps (supplementary figure S1 available at stacks.iop.org/Nano/22/254006/mmedia). Furthermore, those
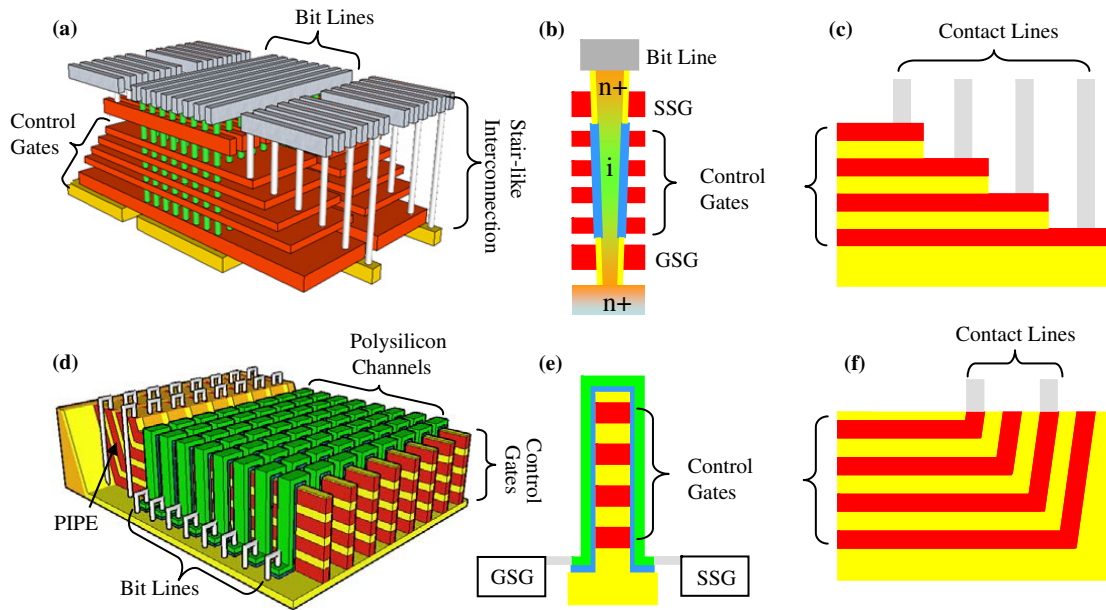
Figure 1. Comparison of 3D NAND structures between BiCS (Toshiba) and VSAT (Our work). (a) Bird's eye view of BiCS. BiCS comprises of vertical NAND strings punched through the multiple stacks of the gate electrode. (b) Cross section of the BiCS memory string. The polysilicon channel plugs into a through-hole, surrounded by control gates (CGs). The select gates (SGs) are embedded in the top and bottom of the vertical string, occupying the Si substrate. (c) Stair-like vertical integration of BiCS. Stacked CGs are connected with contact lines through a stair-like structure, formed by several lithography and dry etching processes. (d) Bird's eye view of the VSAT. The VSAT is a series of vertical NAND strings, featuring a mesa structure and covered by a polysilicon channel. (e) Cross section of a VSAT memory string. Since the VSAT does not embed SGs in the vertical string leaving the Si substrate unoccupied, the procedure to build up the vertical string is simple. (f) PIPE structure for the vertical integration. The PIPE structure requires fewer process steps and less overhead area than stair-like structures. This also provides the same access depth for contact lines, thus leading to an easier via-hole process.

structures turn out to be unsuitable for 3D chip architecture to maximize cell-area efficiency (ratio of memory area to chip area). In this paper, we report a breakthrough to increase memory density in a cost-effective manner by wafer level 3D memory chip architecture, called SMOL (stacked-memory-devices-on-logic). The SMOL has been realized through an innovative 3D memory device of a vertical-stacked-array-transistor (VSAT) [22] and interconnection structure of planarized-integration-on-the-same-plane (PIPE) [20].

2. VSAT and PIPE structure

A VSAT is a series of vertical NAND devices with a polysilicon channel that overcomes the above-mentioned scaling limits and process complexity, and achieves ultra-high-density memory devices. The polysilicon channel covers stacked control gates (CGs, figure 1(d)) and each CG has a double-gate-in-series structure embedding a SONOS layer on both sidewalls (figure 1(e)). The electric current flows horizontally in general from the source-select-gate (SSG) to the ground-select-gate (GSG), but locally up-and-down along the vertical strings. The VSAT memory density is proportional to the number of staked layers, which can be freely increased by depositing extra CG layers without needing advanced and expensive lithography processes. In other words, the effective cell area decreases in reverse proportion to the number of stacked layers and hence the chip area could be reduced by 45% ($=60\% - 60\% \times 1/4$, where 60% is

the ratio of memory area to chip area) in the case of four multiple stacks or 52.5% ($=60\% - 60\% \times 1/8$) in the case of eight multiple stacks. PIPE (figure 1(f)) is a unique interconnection structure providing a more convenient and cost-efficient method than a conventional stair-like structure (figure 1(c)). The PIPE will also impact various crossbar-typed devices [32–37], which have ultimate memory density, to develop much easier and cost-effective interconnections (supplementary figure S2 available at stacks.iop.org/Nano/22/254006/mmedia). We have successfully demonstrated the VSAT prototypes with PIPE structure having a 100 nm feature size (figures 2(b)–(d)). The process starts from creating an oxide mesa structure (figure 2(a)). Next, multiple layers of doped polysilicon for CGs and insulating film are alternately deposited. Afterward, the multi-layer stack is defined into a vertical fin array, and all the CG electrodes are exposed on the same plane through a CMP process to provide easy access for outside connections. The tunneling-oxide, charge-trapping-nitride, and control-oxide films conformally wrapped around the fin array are sequentially deposited, followed by depositing a conformal ultra-thin polysilicon film as the channel material. Finally, a process to pattern the polysilicon into line-shaped channels is carried out. The combined VSAT and PIPE structure offers numerous advantages over other 3D structures such as ultra-high memory density, a simple process sequence, easy integration with peripheral circuits, small overhead area for the vertical interconnection, and highly suppressed short-channel effects (supplementary figure S3 available at stacks.iop.org/Nano/22/254006/mmedia).
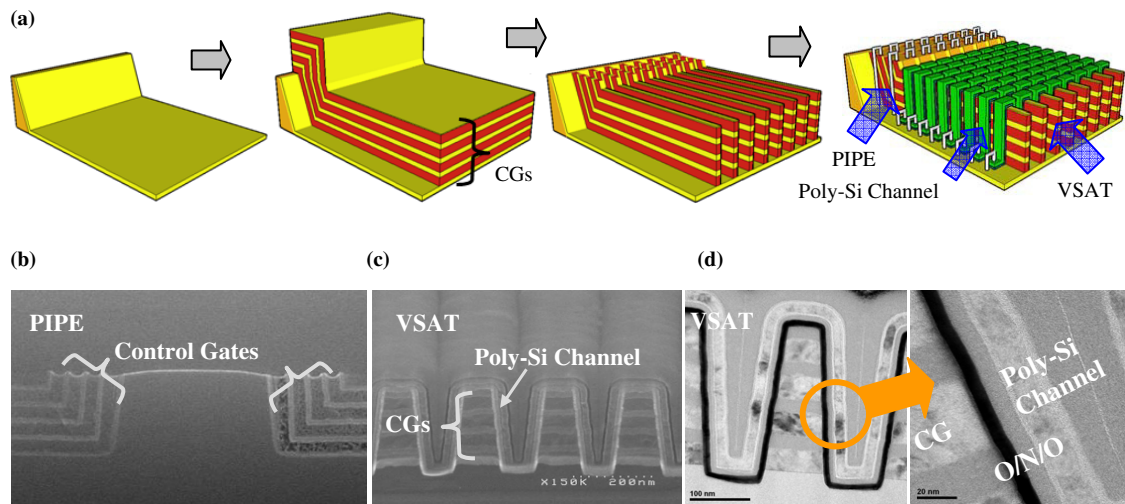
Figure 2. Features of the VSAT structure. (a) Process sequence of VSAT. Multiple layers of gate electrodes and isolating films are deposited over an oxide mesa. The control gates (CGs) are defined through a lithography and dry etching process, followed by a CMP process flattening the CGs. After depositing SONOS and polysilicon films on CGs and separating the channels, an interconnecting process is followed. (b) SEM image of the PIPE structure. A pair of PIPEs is formed on both sides of an oxide mesa, enabling the via-holes to leave out every second CG, thus leading to an easy via-hole process. (c) SEM image of the VSAT. A VSAT with four multiple layers (280 nm high) has been developed at the 100 nm technology node using KrF lithography. (d) TEM images of VSAT. Al_2O_3/nitride/tunneling-oxide are deposited in turn on CGs, finally followed by a 20 nm thick polysilicon film for a channel material.

3. SMOL, 3D memory chip architecture

In a typical 2D architecture, memory arrays and peripheral logic devices are generally located on the same plane above the Si substrate (figure 3(a)) since both devices use single crystalline Si as the channel material. These 2D chips have a cell-area efficiency of approximately 60% and in other words, peripheral logic devices use 40% of the chip area. In order to increase the cell-area efficiency, the 3D vertical-chip architecture is preferred to have the memory and logic cells stacked vertically (figure 3(b)). With this configuration, the VSAT structure can be readily implemented for the 3D chip architecture, SMOL (figures 3(c) and (d)), because the SGs are spatially separated from the memory arrays. The underlying Si substrate can thus be freed up in a VSAT (figure 1(e)) as compared to the BiCS structure in which the Si substrate is utilized as the SGs (figure 1(b)). Accordingly, the peripheral CMOS devices are first built up over the whole chip area together with interconnect lines and landing-pads for vertical interconnection. Stacked-memory-devices are then formed above it. In order to have vertical connections between VSAT and logic devices, the polysilicon channels are connected to the SGs through the landing-pads, while the CGs are connected to the CG-drivers through the landing-pads as well as the PIPE structures (figures 3(c) and (d)).

The SMOL structure with VSATs has many advantages over other stand-alone 3D memory device implementations. The first and main advantage is the increased cell-area efficiency originating from a vertical arrangement of memory and logic devices. Figure 3(d) shows the configuration of a SMOL structure composed of four multiple-stacked layers, and a pair of PIPE structures at both ends of each CG. An impressive cell-area efficiency of more than 95% is achieved,

assuming that the unit block consists of 2 kB/page, 16 vertical stacks per string, and four multiple layers in a vertical stack (supplementary figure S4 available at stacks.iop.org/Nano/22/254006/mmedia). A 5% overhead area is sufficient to build up the PIPE structure with a 50 nm thick CG, 40 nm vertical spacing, and 70° angle on a 100 nm feature size (figure 3(e)). As a result, memory density increases by 35% for the same chip area. Second, the requirement of scaling down logic devices becomes less stringent because the whole Si substrate can be used to configure the peripheral logic devices, which results in lower subthreshold leakage current and thus lower power consumption. Third, the SMOL process sequence is simpler and more cost-effective than the 2D chip architecture, which usually fabricates the 3D memory devices separately from the 2D logic devices, and thus requires additional processing steps for protecting the devices. Furthermore, higher system speed might be possible through the elimination of I/O buffers and with, instead, a direct interface with internal host logic devices in the same chip, when the SMOL technology is realized above microprocessor circuits [38]. In this study, a prototype SMOL structure has been successfully developed with a feature size of 100 nm, fabricating VSAT above the pre-fabricated logic devices. Tungsten is used as the interconnection material for logic devices to endure the subsequent high processing temperature involved in fabricating VSAT devices. Multiple layers of n-type doped polysilicon and oxide thin films are deposited on an oxide buffer layer of 300 nm thick (figure 3(f)). Next, the SMOL prototype is constructed using the fabrication steps for the VSAT (figure 2(a)) and demonstrates highly integrated 3D memory on logic chip architecture (figure 3(g)).
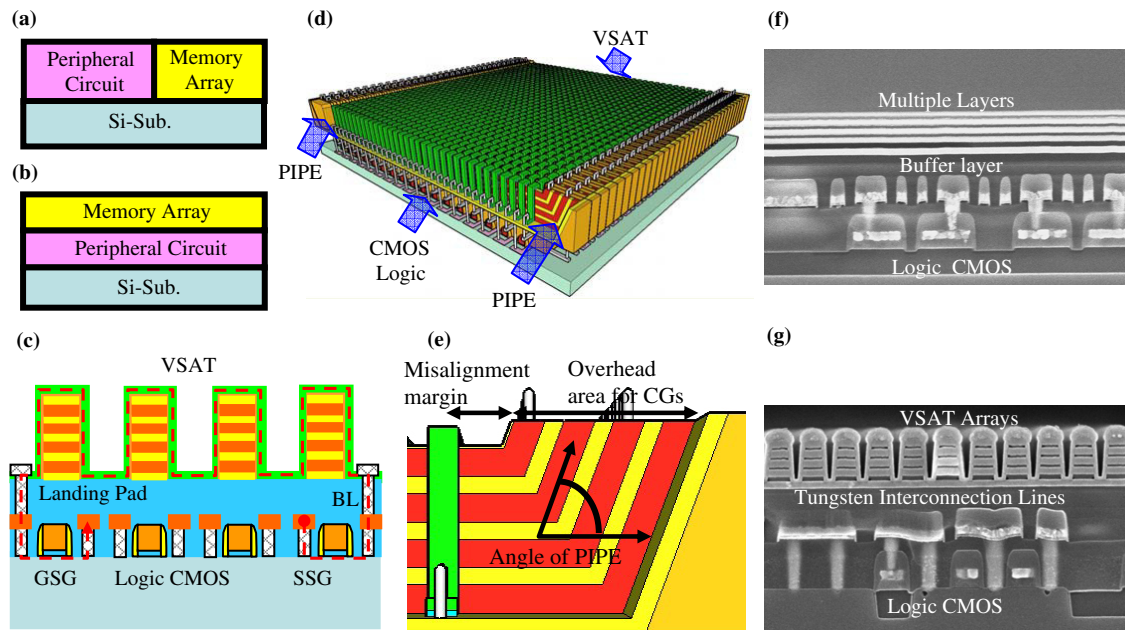
Figure 3. Features of SMOL structure. (a) 2D memory chip architecture. Memory arrays are normally based on a Si substrate like peripheral CMOS devices which occupy almost 40% of a chip's area. (b) 3D memory chip architecture. Cell-area efficiency can be maximized through the 3D chip architecture arranging the memory part over the peripheral CMOS part. (c) The basic concept of SMOL. CMOS devices are based on the whole chip area first, and then memory devices of VSATs are built up above the CMOS devices. A polysilicon channel is connected to SGs through the landing-pad. The red broken line shows the electric current path from SSG to GSG through VSAT arrays. (d) Bird's eye view of SMOL. SMOL allocates the memory devices on the peripheral CMOS devices. Pairs of PIPE are formed at the end of CGs and connected to a CG's driver circuit located at the lower part. The polysilicon channels are directly connected to the SGs located in the block's edge of the lower part. (e) The overhead area in PIPE. The overhead area of PIPE depends on the number of multiple layers, the angle of PIPE, and the misalignment tolerance. (f) SEM image of SMOL after depositing the multiple layers. Four multiple layers were deposited on a 300 nm thick oxide buffer layer above the CMOS devices. (g) SEM image of the final SMOL structure. A prototype of SMOL has been developed building up VSATs with a feature size of 100 nm above CMOS devices with a feature size of 150 nm, illustrating the capability of the processing.

4. Electrical performance

Although polysilicon is widely used as a channel material in 3D devices, there is still a critical concern about its electrical performance as a FET channel due to the trapping sites at the polysilicon grain boundaries. In order to lower the device threshold voltage (V_{th}) and improve subthreshold characteristics, an ultra-thin polysilicon film has been employed [18] as it reduces the polysilicon volume and total number of traps. With an ultra-thin polysilicon film of 20 nm thick and a hydrogen annealing process that reduces the total number of traps, the device electrical performance has been significantly improved with a lowered V_{th} of 1.5 V (from 6.0 V), a reduced subthreshold slope of 300 mV dec^{-1} (from 800 mV dec^{-1}), and an increased drive current of 1.3 A m^{-1} (from 0.3 A m^{-1}) (figures 4(a) and (b) and supplementary figure S5 available at stacks.iop.org/Nano/22/254006/mmedia). Memory operations of VSAT are similar to those of the conventional SONOS Flash memory through the trapping or de-trapping electrons in the nitride layer through FN tunneling current. However, since VSAT has a floating body structure, a negative bias on the CG is required in an erasing operation. A single pulse of ±14 V has been applied to program and erase the device, respectively. After a 100 ms programming and erasing operation cycle, the V_{th} shifts by as much as 4 V, which is also an excellent window (figures 4(d)–(f)).

5. Results of device simulation

The source–drain region of a VSAT has an identical doping level to the channel region because no intentional doping has been introduced into the former, unlike in conventional FETs. The electrons in the source–drain region are induced by the fringing electric field (figure 5(a)) of CGs, which electrically connect the individual channels together as one conducting path (supplementary figure S6 available at stacks.iop.org/Nano/22/254006/mmedia). The channel doping level and vertical distance between WLs are therefore the crucial parameters for desired electrical performance. A larger vertical spacing yields less interference yet it results in larger parasitic resistance in the source–drain region, which might even disconnect the channels. MEDICI™ simulations have been carried out for varying dopant types and doping levels in the polysilicon film, while fixing the vertical spacing to 50 nm in order to ensure a small cell-to-cell interference. The simulation results show that the electrical characteristics are uniform through a wide range of doping levels from 10^{16} cm^{-3} of boron to 10^{16} cm^{-3} of phosphorus (figures 5(b) and (c)), even though the parasitic resistance increases for heavily doped p-type cases and leakage current rapidly increases in heavily doped n-type cases (figure 5(c)). An ultra-thin polysilicon film makes this wide doping window possible because the total amount of charge ($Q_{total} = N_{doping} \times t_{body}$) is small even with high doping levels. This in turn yields a small
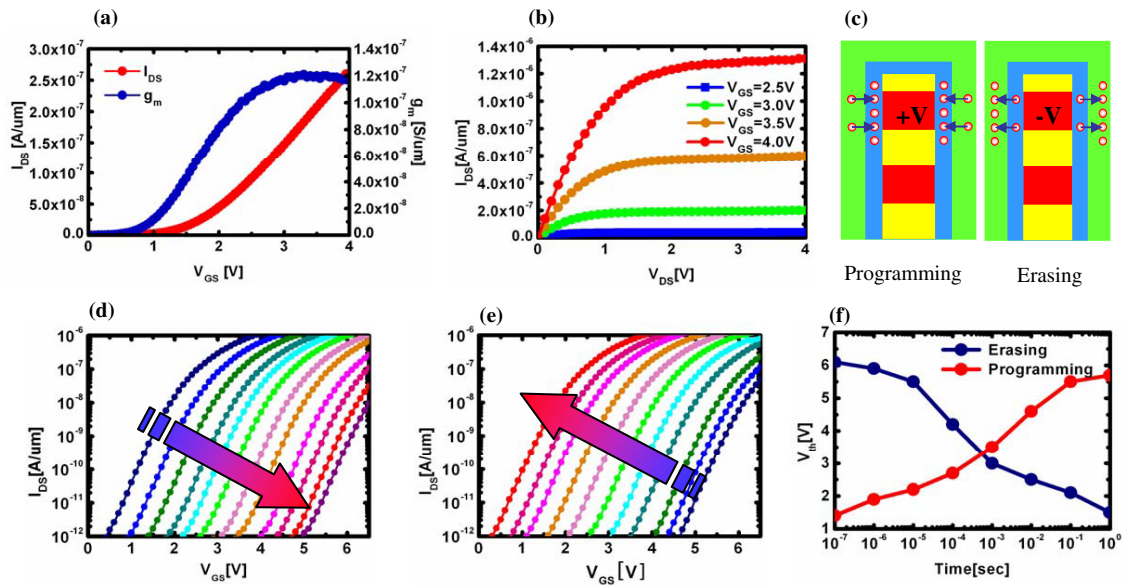
Figure 4. Electrical performance of VSAT. (a) V_{GS}–I_{DS} plot. DC performance is improved by adopting a thin polysilicon channel and a hydrogen annealing process, showing 1.5 V of V_{th}, 300 mV dec^{-1} of subthreshold slope, and 15 cm^2 V^{-1} s^{-1} of mobility extracted from the maximum transconductance. (b) V_{DS}–I_{DS} plot. 1.3 μA μm^{-1} of drive current is achieved at $V_{GS} = 4.0$ V. (c) Mechanism of programming or erasing. Electrons move in either the forward or reverse direction between a channel and a trapping layer of nitride via the polarity of the gate bias. Trapping or de-trapping electrons in a nitride film shifts the threshold voltage of the device and serves as the data storage mechanism. (d) Memory functions. Positive bias on gates pulls electrons from the channel to the trapping layer, and thus V_{th} moves up. (e) Negative bias pushed electrons from the trapping layer to the channel, and V_{th} moves down. (f) V_{th} changes by as much as 4 V after a 100 ms programming and erasing cycle.
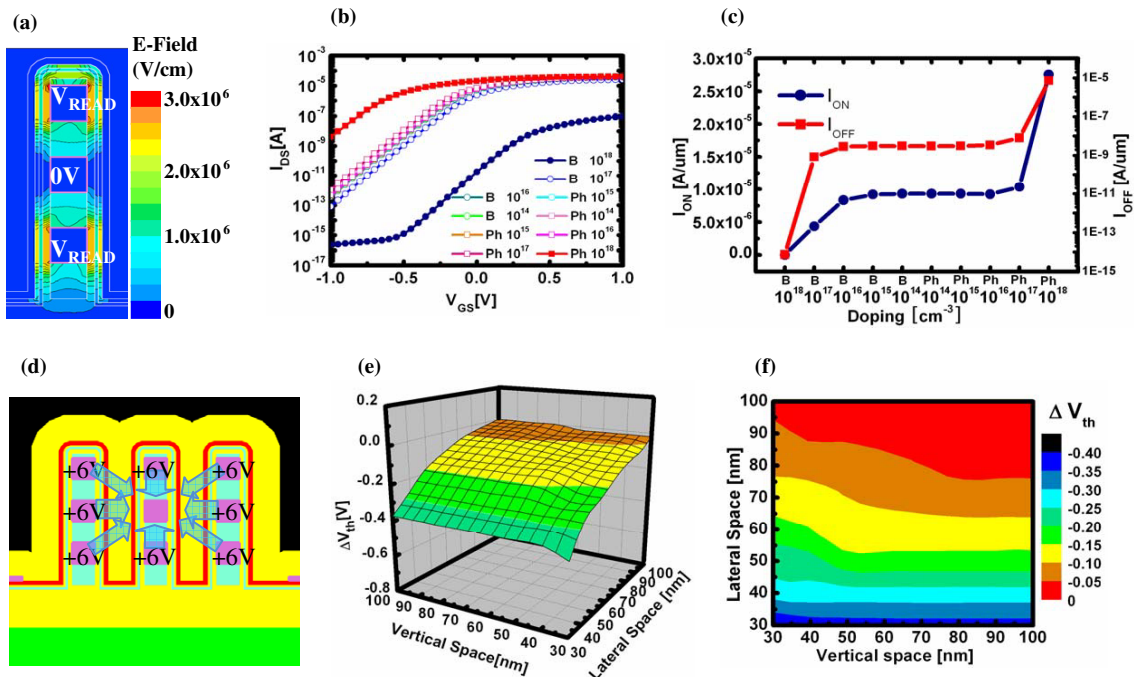

Figure 5. Device simulations. (a) Fringing electric field in the source–drain region. The electric field affects the source–drain region through the fringing capacitance, and induces electrons, electrically connecting the whole channel. (b) V_{th} depending on the channel doping levels simulated by MEDICI. V_{th} varies less than 50 mV under a wide window of doping levels. (c) I_{ON}–I_{OFF} characteristics simulated by MEDICI. I_{ON} and I_{OFF} shows stable performance from B 10^{16} to Ph 10^{16} cm^{-3}, although it shows highly conducting or non-conducting characteristics in extremely highly doped cases. (d) Interference mechanism in VSATs. A V_{th} shift occurs on the center cell because of the neighboring cells with an applied bias of VREAD. (e) and (f) V_{th} shift by interference simulated by MEDICI. The lateral spacing is more sensitive than the vertical spacing, owing to the larger coupling capacitance. VSAT can be scaled down to 40 nm vertically and 50 nm laterally maintaining 0.25 V of V_{th} shift.

potential change ($V = Q_{\text{total}}/C_{\text{ox}}$) and thus a stable operation. Finally, the interference between neighboring cells in VSAT is examined because it would limit the proximity between cells, and thus the ultimate memory density and scalability. Through MEDICI™ simulations, direct interference effects have been studied by monitoring the V_{th} shift induced by the neighboring CGs' potential (figure 5(d)). The amount of interference is proportional to the coupling capacitance between the channel and neighboring CGs. The lateral coupling is stronger than the vertical coupling since the CGs and channels face each other, which constitutes a larger coupling area. The amount of V_{th} shift is estimated to be 0.25 V, an acceptable number by the industrial standard, with a 50 nm lateral spacing and 40 nm vertical spacing (figures 5(e) and (f)). This result strongly supports the VSAT strategy to increase the memory density by staking more layers, which is manufactured using only relatively low-cost lithography, deposition, and etching processes.

6. Conclusion

A novel SMOL structure has been successfully developed through a simple and cost-effective method. The cell-area efficiency of more than 95% can be achieved through the SMOL structure with a feature size of 100 nm. Electrical performance of the polysilicon channel has been dramatically improved by adopting an ultra-thin film and hydrogen annealing process. MEDICI™ simulations exploring interference and channel doping effects show that the SMOL structure shows many desirable memory characteristics. The advantages of the SMOL architecture make it a viable candidate for low-cost and high-density memory devices. This technology is compatible with the CMOS process and is also applicable to various emerging memory devices.

References

[1] Shimizu K *et al* 1997 A novel high-density 5F^2 NAND STI cell technology suitable for 256 Mbit and 1 Gbit flash memories *IEDM '97: Technical Digest., Int. Electron Devices Mtg* pp 271–4

[2] Kim K 2005 Technology for sub-50 nm DRAM and NAND flash manufacturing *IEDM Technical Digest. IEEE Int. Electron Devices Mtg* pp 323–6

[3] Shin Y 2005 Non-volatile memory technologies for beyond 2010 *Digest of Technical Papers. 2005 Symp. VLSI Circuits* pp 156–9

[4] Hwang C-G 2006 New paradigms in the silicon industry *IEDM '06: Int. Electron Devices Mtg* pp 1–8

[5] Kim K 2006 Memory technologies for 50 nm and beyond *ICSICT '06: 8th Int. Conf. Solid-State and Integrated Circuit Technology* pp 685–8

[6] Kim K *et al* 2006 Future outlook of NAND flash technology for 40 nm node and beyond *IEEE NVSMW 2006: 21st Non-Volatile Semiconductor Memory Workshop* pp 9–11

[7] Kim K *et al* 2007 Memory technologies for sub-40 nm node *IEDM 2007: IEEE Int. Electron Devices Mtg* pp 27–30

[8] Kim K 2008 Future memory technology: challenges and opportunities *VLSI-TSA 2008 Int. Symp. VLSI Technology, Systems and Applications* pp 5–9

[9] Park K-T *et al* 2008 A zeroing cell-to-cell interference page architecture with temporary LSB storing and parallel MSB program scheme for MLC NAND flash memories *IEEE J. Solid-State Circuits* **43** 919–28

[10] Santo B 2009 25 microchips that shook the world *IEEE Spectrum* **46** 34–43

[11] SAMSUNG SSD versus HDD

[12] Pon H *et al* 2007 A NAND flash PC platform read write cache *22nd IEEE Non-Volatile Semiconductor Memory Workshop* pp 21–2

[13] Pon H 2008 NAND flash read/write cache directions for the personal computing platform *ICSICT 2008: 9th Int. Conf. Solid-State and Integrated-Circuit Technology* pp 815–8

[14] Lee D *et al* 2009 PDC-NH: popular data concentration on NAND flash and hard disk drive *10th IEEE/ACM Int. Conf. on Grid Computing* pp 196–200

[15] Kim J-H *et al* 2009 A methodology for extracting performance parameters in solid state disks (SSDs) *MASCOTS '09: IEEE Int. Symp. on Modeling, Analysis & Simulation of Computer and Telecommunication Systems* pp 1–10

[16] Pirovano A *et al* 2010 Integrated circuits: memory grows up *Nat. Nanotechnol.* **5** 177–8

[17] Jung S-M *et al* 2006 Three dimensionally stacked NAND flash memory technology using stacking single crystal Si layers on ILD and TANOS structure for beyond 30 nm node *IEDM '06: Int. Electron Devices Mtg* pp 1–4

[18] Fukuzumi Y *et al* 2007 Optimal integration and characteristics of vertical array devices for ultra-high density, bit-cost scalable flash memory *IEDM 2007: IEEE Int. Electron Devices Mtg* pp 449–52

[19] Tanaka H *et al* 2007 Bit cost scalable technology with punch and plug process for ultra high density flash memory *IEEE Symp. on VLSI Technology* pp 14–5

[20] Kim J *et al* 2008 Novel 3D structure for ultra high density flash memory with VRAT (vertical-recess-array-transistor) and PIPE (planarized integration on the same plane) *Symp. on VLSI Technology* pp 122–3

[21] Jang J *et al* 2009 Vertical cell array using TCAT(terabit cell array transistor) technology for ultra high density NAND flash memory *Symp. on VLSI Technology* pp 192–3

[22] Kim J *et al* 2009 Novel vertical-stacked-array-transistor (VSAT) for ultra-high-density and cost-effective NAND flash memory devices and SSD (solid state drive) *Symp. on VLSI Technology* pp 186–7

[23] Katsumata R *et al* 2009 Pipe-shaped BiCS flash memory with 16 stacked layers and multi-level-cell operation for ultra high density storage devices *Symp. on VLSI Technology* pp 136–7

[24] Kim W *et al* 2009 Multi-layered vertical gate NAND flash overcoming stacking limit for terabit density storage *Symp. on VLSI Technology* pp 188–9

[25] Park J-H *et al* 2004 8 Gb MLC (multi-level cell) NAND flash memory using 63 nm process technology *IEDM Technical Digest. IEEE Int. Electron Devices Mtg* pp 873–6

[26] Park K-T *et al* 2006 A high cost-performance and reliable three-level MLC NAND flash memory using virtual page cell architecture *IEEE NVSMW 2006: 21st Non-Volatile Semiconductor Memory Workshop* pp 34–5

[27] Park Y *et al* 2006 Highly manufacturable 32Gb multi–level NAND flash memory with 0.0098 μm^2 cell size using TANOS(Si-oxide-Al$_2$O$_3$-TaN) cell technology *IEDM '06: Int. Electron Devices Mtg* pp 1–4

[28] Shibata N *et al* 2007 A 70 nm 16Gb 16-level-cell NAND flash memory *IEEE Symp. on VLSI Circuits* pp 190–1

[29] Chang L A 2008 Hybrid approach to NAND-flash-based solid-state disks *IEEE Trans. on Computers* pp 1337–49

[30] Ki-Tae P *et al* 2006 A high cost-performance and reliable 3-level MLC NAND flash memory using virtual page cell architecture *IEEE NVSMW 2006: 21st Non-Volatile Semiconductor Memory Workshop* pp 34–5

[31] Chiang M-L *et al* 2008 A new FTL-based flash memory management scheme with fast cleaning mechanism *ICESS '08: Int. Conf. Embedded Software and Systems* pp 205–14

[32] Luyken R J and Hofmann F 2003 Concepts for hybrid CMOS-molecular non-volatile memories *Nanotechnology* **14** 273

[33] Choi Y-H and Kim Y K 2004 A nanoscale scalable memory architecture for molecular electronics *Nanotechnology* **15** S639

[34] Deng J *et al* 2007 Metallization for crossbar molecular devices *Nanotechnology* **18** 155202

[35] Vontobel P O *et al* 2009 Writing to and reading from a nano-scale crossbar memory based on memristors *Nanotechnology* **20** 425204

[36] Yun D K *et al* 2009 Mass fabrication of resistive random access crossbar arrays by step and flash imprint lithography *Nanotechnology* **20** 445305

[37] Jeong H Y *et al* 2010 A low-temperature-grown TiO_2-based device for the flexible stacked RRAM application *Nanotechnology* **21** 115203

[38] Brewer J E and Gill M 2008 Nonvolatile memory technologies with emphasis on flash *A Comprehensive Guide to Understanding and Using Flash Memory Devices* (*IEEE Press Series on Microelectronic Systems*) (Picataway, NJ: IEEE) pp 375–6